ADVANCED HEALTHCARE MATERIALS
www.advhealthmat.de

E-Suture: Mixed-Conducting Suture for Medical Devices

Onni J. Rauhala, Liang Ma, Duncan J. Wisniewski, Shan Shao, Brandon Schumacher, Jose Ferrero Lopez, Mara Kaspers, Zifang Zhao, Jennifer N. Gelinas, and Dion Khodagholy**

Modern implantable bioelectronics demand soft, biocompatible components that make robust, low-impedance connections with the body and circuit elements. Concurrently, such technologies must demonstrate high efficiency, with the ability to interface between the body's ionic and external electronic charge carriers. Here, a mixed-conducting suture, the e-suture, is presented. Composed of silk, the conducting polymer poly(3,4-ethylenedioxythiophene) polystyrene sulfonate (PEDOT:PSS), and insulating jacketing polymers,the resulting e-suture has mixed-conducting properties at the interface with biological tissue as well as effective insulation along its length. The e-suture can be mechanically integrated into electronics, enabling the acquisition of biopotentials such as electrocardiograms, electromyograms, and local field potentials (LFP). Chronic, in vivo acquisition of LFP with e-sutures remains stable for months with robust brain activity patterns. Furthermore, e-sutures can establish electrophoretic-based local drug delivery, potentially offering enhanced anatomical targeting and decreased side effects associated with systemic administration, while maintaining an electrically conducting interface for biopotential monitoring. E-sutures expand on the conventional role of sutures and wires by providing a soft, biocompatible, and mechanically sound structure that additionally has multifunctional capacity for sensing, stimulation, and drug delivery.

1. Introduction

Implantable bioelectronics are becoming established components of advanced healthcare devices, providing a variety of clinical diagnostics and interventions.[1–3] Such devices offer local, personalized, and even responsive electrical stimulation to the heart, brain, and nerves to manage chronic medical conditions.[4–9] Similar to any electronic device, they require wires and interconnects for effective transfer of power and data along their circuits. Several implantable devices that target viscera or deep brain structures separate the active tissue interface from the main electronics enclosure, which is more superficially located, necessitating use of a length of wire to connect the device components.[7,10,11] This approach enables minimally invasive procedures that reduce disruption to sensitive structures. For instance, deep brain stimulation (DBS) is accomplished via the implantation of a flexible multi-electrode array in target brain structures and subcutaneous placement of the main electronic circuitry and battery in the chest. These modules are connected using wires that pass through the scalp, neck, and shoulder. For such device designs, the stability of the connection is critical for safe and reliable function. Wires used for this purpose are conventionally composed of a core of an inert and malleable metal (such as stainless steel) to serve as the conductor and a coating of U.S.P. class VI plastic to form the insulating jacket. Although such wires demonstrate reliable signal conduction, their rigidity and overall thickness can lead to discomfort, tissue adhesions, and limitations to permitted movements for patients.[12] Furthermore, because these metals have high electrochemical impedance relative to the surface area, they typically require a connector to interface front-end sensors, increasing the bulkiness of the implant.[13]

Localized drug delivery is another desirable feature of bioelectronic devices because this approach improves anatomical drug targeting, reduces systemic side effects, and eliminates any volumetric pressure on the target tissue resultant of vehicular fluids.[14–17] However, due to the complexity of establishing a sterile and safe molecular conduit from the outside to the inside of the body, such devices are not yet widely utilized. The organic electronic ion pump (OEIP), an electrophoresis-based device that can transport charged drug molecules, is a promising technology for the local delivery of drugs without the exchange of fluids.[18–20] These devices are typically fabricated on a planar plastic substrate to provide the required mechanical flexibility for interfacing with biological tissue. However, drugs must often be delivered over

O. J. Rauhala, D. J. Wisniewski, Z. Zhao, D. Khodagholy
Department of Electrical Engineering
Columbia University
New York 10027, USA
E-mail: dk2955@columbia.edu
L. Ma, M. Kaspers, J. N. Gelinas
Department of Biomedical Engineering
Columbia University
New York 10027, USA
E-mail: jng2146@cumc.columbia.edu
S. Shao, B. Schumacher, J. F. Lopez, J. N. Gelinas
Department of Neurology
Columbia University Irving Medical Center
New York 10032, USA

The ORCID identification number(s) for the author(s) of this article can be found under https://doi.org/10.1002/adhm.202302613

DOI: 10.1002/adhm.202302613

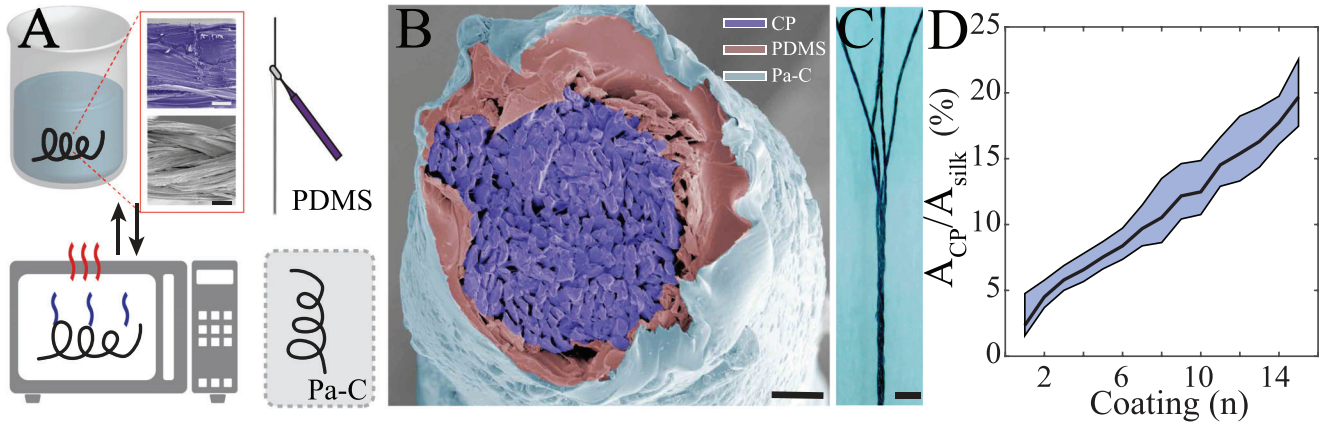

Figure 1. Structural, material, and electrical properties of the e-suture. A) Schematic of the e-suture fabrication process involving repetitive dip-coating cycles of washed sutures in a PEDOT:PSS dispersion, followed by jacketing of the coated suture by hydrophobic polymers (PDMS and Pa-C; Experimental Section). B) Colorized, cross-sectional scanning electron microscopy (SEM) image of the e-suture, showing PEDOT:PSS (conductive polymer, CP)-coated individual silk threads (purple) as well as the insulating PDMS (red) and Pa-C (blue) layers. Scale bar 50 µm. C) Optical micrograph of four e-sutures braided to form a single cable (tetrode). Scale bar 1 mm. D) Ratio of cross-sectional area of the conducting polymer versus silk as a function of number of coating cycles for a 150 µm diameter suture (n = 3, mean ± sd).

a longer physical distance in the body than what is possible to achieve by conventional lithographical patterning.[21] Therefore, there is a significant need for biocompatible, flexible, implantable interconnects with the ability to serve as electrical and chemical conduits.

Here we show that poly(3,4-ethylenedioxythiophene) polystyrene sulfonate (PEDOT:PSS) coated, mixed-conducting silk sutures, e-sutures, provide an organic, highly conductive, soft and biocompatible alternative to metallic wiring in bioelectronic devices with functionalities for biopotential signal acquisition, stimulation, and drug delivery. The e-suture retains these beneficial properties in physiological environments over an extended period of time due to an effective insulating jacket made of polydimethoxysilane (PDMS) and parylene-C (Pa-C). We highlight the potential of e-sutures in localized drug delivery via an electrophoretic-based device that can deliver cations without the need for a vehicular liquid while maintaining an electrically conducting interface with the target electrolyte. In addition, e-sutures can be utilized as interface electrodes in multiple types of electrophysiological recording and stimulation procedures via robust mechanical connections to circuits. Finally, e-sutures can serve as chronic neural interface devices and provide high-quality local field potential (LFP) over the course of months. Our results illustrate the capacity of organic materials to simplify and expand bioelectronic device design with potential clinical applicability.

2. Structural, Material, and Electrical Properties of E-Sutures

To create e-sutures, we began by washing braided multifilament silk sutures in baths of soapy water, isopropanol, and acetone to remove organic contaminants. We then soaked the sutures in a highly conductive dispersion of PEDOT:PSS (see Experimental Section for details), followed by drying in a convection oven at atmospheric pressure. Once suitable conductivity was obtained through the addition of multiple PEDOT:PSS coats, an insulation layer was added to create a jacketed e-suture. PDMS was chosen as the first layer of insulation to control elasticity and establish a hydrophobic surface.[22] An outer layer of Pa-C was then deposited conformally using chemical vapor deposition[23] to eliminate any pin-holes (**Figure 1**A,B). This insulation process was robust along the length of the e-suture, permitting braiding into multiconductor cables with minimal cross-talk and absence of short circuiting (Figure 1C). The process of generating an e-suture mildly reduced the tensile strength of the silk, but the value remained comparable to other common surgical suture materials (i.e., nylon), indicating preserved mechanical properties of the e-suture for conventional clinical applications (Figure S1, Supporting Information). To characterize the PEDOT:PSS deposition process, we measured the e-sutures electrical resistance over 1 cm at several points and calculated the cross-sectional area of conducting polymer (A_{CP}) required to generate these values (Figures S1–S3, Supporting Information). We assumed the nominal conductivity of PEDOT:PSS in thin-film configuration to be 800 S cm^{-1}.[24–26] Comparing the A_{CP} to the known cross-sectional area of the original silk suture (A_{silk}), we found that the calculated amount of PEDOT:PSS increased linearly with number of coats added, suggesting that the conductive polymer dispersion diffused effectively and additively into the braided structure of the silk during the coating process (Figure 1D; Figure S2,3, Supporting Information). Furthermore, measuring the resistance across progressively longer distances along the e-suture yielded a directly proportional increase in R (Ω), indicating uniform conduction properties and thus polymer coating along the entire suture (Figure S3, Supporting Information).

3. E-Suture Establishes a Cross-Talk Free, Low Impedance Interface over an Extended Time Period

Next, we determined the electrical and electrochemical performance of e-sutures serving as electrophysiological interfaces. We integrated multiple e-sutures with conventional planar

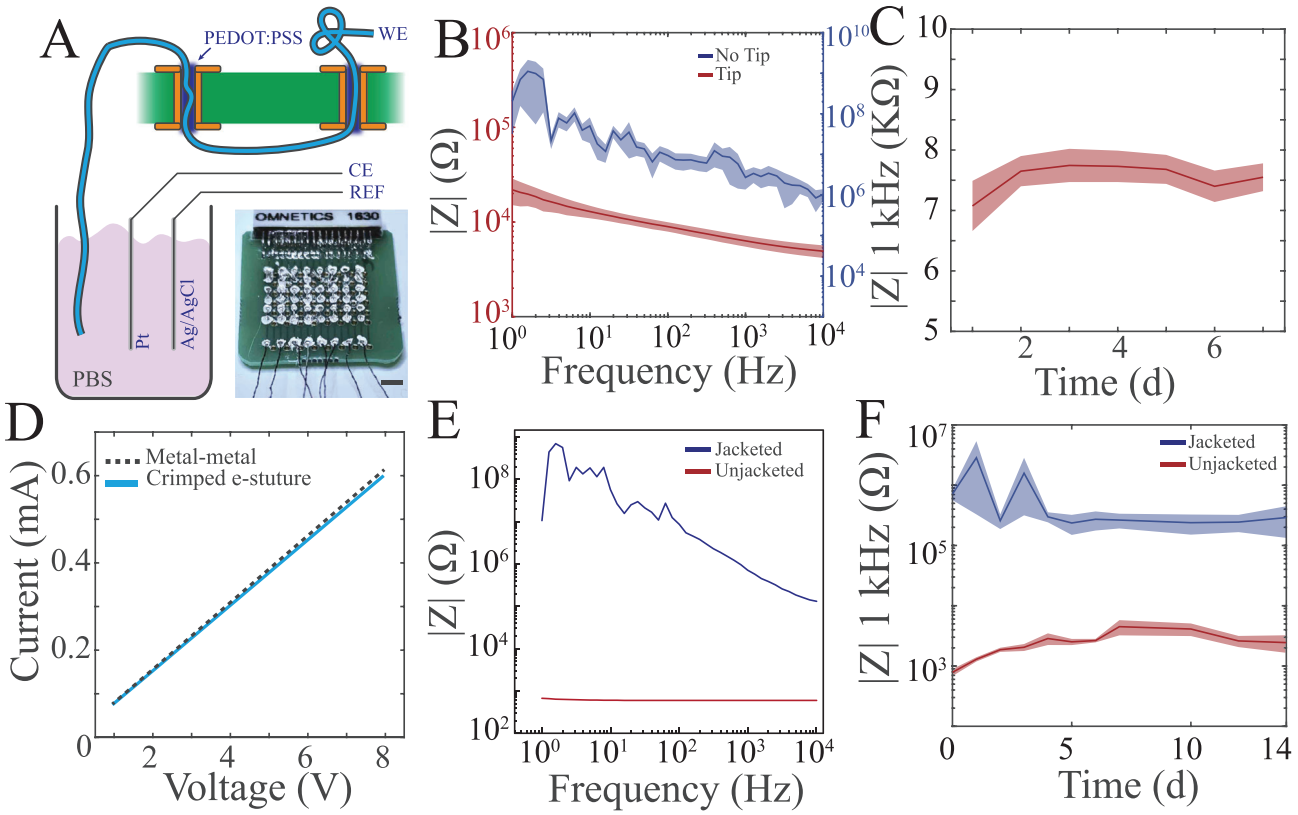

Figure 2. E-sutures provide a low impedance, cross-talk free interface with reliable electrical integration over an extended period of time. A) Cross-sectional schematic of the potentiostat-mode electrochemical impedance spectroscopy (EIS) of an e-suture integrated with a printed circuit board for facile integration with planar electronics (left). Optical micrograph of a neural interface device composed of multiple e-sutures as recording electrodes and interconnects (bottom right). Scale bar 1 mm. B) Comparison of the EIS of an exposed e-suture tip, acting as an electrode (blue, mean ± standard error of measurement (s.e.m.)) versus a completely insulated suture with no exposed tip (red, mean ± s.e.m.). C) Mean impedance of e-suture electrode tips at 1 kHz over a course of one week while immersed in PBS (mean ± s.e.m.). D) Current delivery through an e-suture versus a metal wire in a mechanical crimp connection with a metal contact. E) Sample trace EIS of a jacketed e-suture (blue) versus unjacketed e-suture (red) in a PBS bath. F) Mean impedance at 1 kHz of jacketed e-sutures versus uninsulated e-suture over the course of two weeks while immersed in PBS (mean ± s.e.m.).

electronics by passing them through vertical interconnect accesses (vias) of a printed circuit board (PCB) and mechanically fastened them using simple knots. This method generated a multi-channel sensing device with independently accessible e-sutures functioning as electrodes through their exposed tips (**Figure** 2A). Electrochemical impedance spectroscopy (EIS) on the exposed tips revealed low impedance values that were comparable to those reported with solution-processed[27–29] or electrochemically deposited[30–33] conducting polymers on metal pads. In contrast, the jacket of the e-suture was found to be a robust insulator, providing a strong ion barrier and high impedance (Figure 2B). These impedance values were constant over the course of a full week of continuous immersion in phosphate buffered saline (PBS), indicating stability in physiologic conditions (Figure 2C). The jacketing also resulted in a uniformly high impedance when measured along the length of the e-suture and provided sufficient mechanical stability required for repetitive suturing of synthetic skin models without degradation of the insulating capacity as measured by EIS (Figures S4 and S5, Supporting Information). We further observed that it was possible to establish a reliable, low contact-resistance electrical junction between an e-suture and metal-based electrical connectors, allowing for integration with conventional electronics (Figure 2D). To determine applicability of e-sutures for long-range data or power interconnects, we evaluated the consistency of the impedance over the entire length (~70 cm) of the e-suture using EIS. The jacketed suture displayed significantly elevated and stable impedance compared to an unjacketed suture across a two-week period of immersion in PBS (Figure 2E,F). Taken together, these results corroborate the conclusion of the e-suture functioning as a low impedance electrical interface with a uniform, pin-hole free insulation layer.

4. E-Suture Permits Electrophoretic-Based Drug Delivery

Given the mixed-conducting properties of PEDOT:PSS and hydrophilic nature of silk,[34–36] we hypothesized that it would be possible to create an electrophoresis-based drug delivery device using an e-suture as an ion delivery channel and electrophysiological sensor simultaneously. This approach is distinct from the established OEIP system, where the drug delivery pathway serves only as an ion conductor (**Figure** 3A, top). To achieve this e-suture

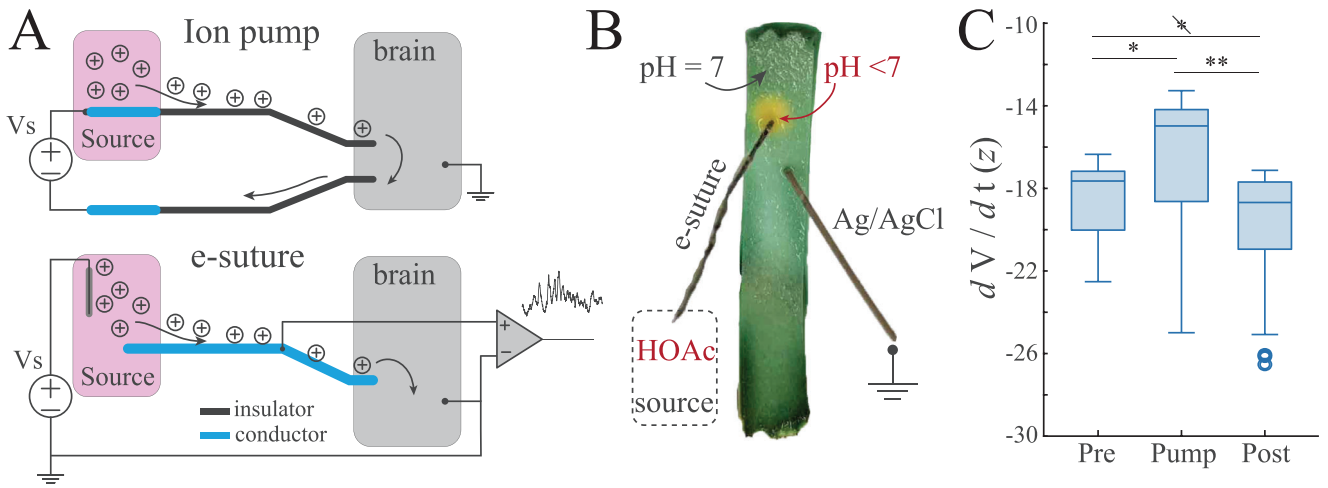

Figure 3. E-sutures enable local delivery of cations. A) Schematic illustrating the difference between a conventional organic electrical ion pump (OEIP) and e-suture-based drug delivery. Wiring diagram of an OEIP with ohmic contact of source electrode to supply voltage (top). Note that there is no ability to perform biopotential recordings in this set-up. Wiring diagram of e-suture with conducting electrode that can serve as a drug delivery conduit and recording electrode (bottom). Note the e-suture is not electrically connected to the voltage supply. B) Optical image captured during operation of e-suture delivering protons to a PBS-soaked pH indicator strip. Note the indicator is green (pH = 7) except for the local area in the vicinity of the e-suture, which is yellow, indicating lower pH due to delivery of H^+. C) E-suture induced epileptic sharp waves/spikes by K+ infusion as quantified by z-scored negative derivative values (n = 36 , 37, 35 events for Pre, Pump and Post, respectively). Omnibus Kruskal-Wallis test for e-suture recordings: $\chi^2 = 24.882$, $p < 0.001$. Horizontal bars indicate statistically significant differences from post hoc Dunn-Sidak corrected multiple comparison tests (** = $p < 0.001$, * = $p < 0.05$).

multifunctionality, we established the e-suture itself at a floating potential (i.e., no ohmic contact with the supply or ground potential; Figure 3A, bottom) and used comparatively larger electrodes as voltage and ground to create a potential gradient across the e-suture from the source reservoir to the target tissue. We tested this design by pumping protons (H^+) from a 1 mM acetic acid (CH_3COOH) source reservoir. At the target, we soaked a pH strip with PBS to allow local monitoring of pH at the vicinity of the e-suture tip. By applying a DC potential between the source reservoir and the target PBS bath, we were able to effectively pump protons to the target as indicated by the color change of the pH strip around the e-suture tip (Figure 3B). To assess the e-suture-based ion pump in vivo, we performed a standalone acute recording from an adult rat under anesthesia where we delivered potassium (K+) to the brain and simultaneously recorded the local field potential (LFP) from the same e-suture delivering the K+. We confirmed the successful ion delivery by measuring the current flow through the pump system and by c potassium-induced epileptic sharp waves/spikes in the LFP under anesthesia (Figure 3C; Figure S6, Supporting Information). Overall, it is possible to deploy e-suture technology for localized drug delivery while maintaining the electrical conductivity of the e-suture for the purpose of biopotential recordings.

5. E-Suture Enables a Minimally Invasive Electrophysiologic Interface

We assessed the ability of e-sutures to function as in vivo electrophysiologic sensors and stimulators. We first established a non-invasive interface to record surface electrocardiography (ECG) in a mouse pup (postnatal day 6). Two e-sutures were placed on the skin of a mouse pup over the heart to form a differential recording electrode pair. Due to the flexibility of the silk, we were able to secure the e-sutures onto the skin using soft, air permeable medical tape with no further chemical adhesive (**Figure 4A**). The e-sutures were then crimped to a conventional metal-wire screw-connector for interfacing with a traditional amplifier. The e-sutures effectively tracked the mouse pup's heart rate during anesthesia with hypothermia and throughout anesthesia recovery, demonstrating the expected recovery[37] from 1 beat per second (bps) to a stable 5 bps (Figure 4A,B).

Next, we determined the electrical stimulation capability of e-sutures by interfacing with the peripheral nervous system. A selectively uninsulated e-suture (see Methods for details) wrapped around an exposed sciatic nerve enabled direct nerve stimulation, mimicking a nerve cuff stimulating electrode (Figure 4C). We accomplished similar muscular stimulation without requiring an open surgical procedure by using two pairs of e-sutures as bipolar stimulating and recording electrodes. These e-sutures were inserted into the hindleg of an anesthetized adult rat using a hypodermic needle as an insertion cannula (Figure 4D). The stimulating e-sutures delivered current sufficient to evoke observable muscle contraction that was quantified by the electromyogram (EMG) acquired by the recording e-sutures (Figure 4E). Titration of stimulation current generated EMG potentials that increased in amplitude following a sigmoidal curve (Figure 4F; Figure S7, Supporting Information). These results demonstrate the ability of e-sutures to effectively interface with electrically active tissue for recording and stimulation purposes.

6. E-Sutures Provide High-Resolution Chronic In Vivo Electrophysiology

We then deployed the e-suture as an in vivo neural interface device to perform high-spatiotemporal resolution chronic electrophysiologic recordings from freely moving animals. We

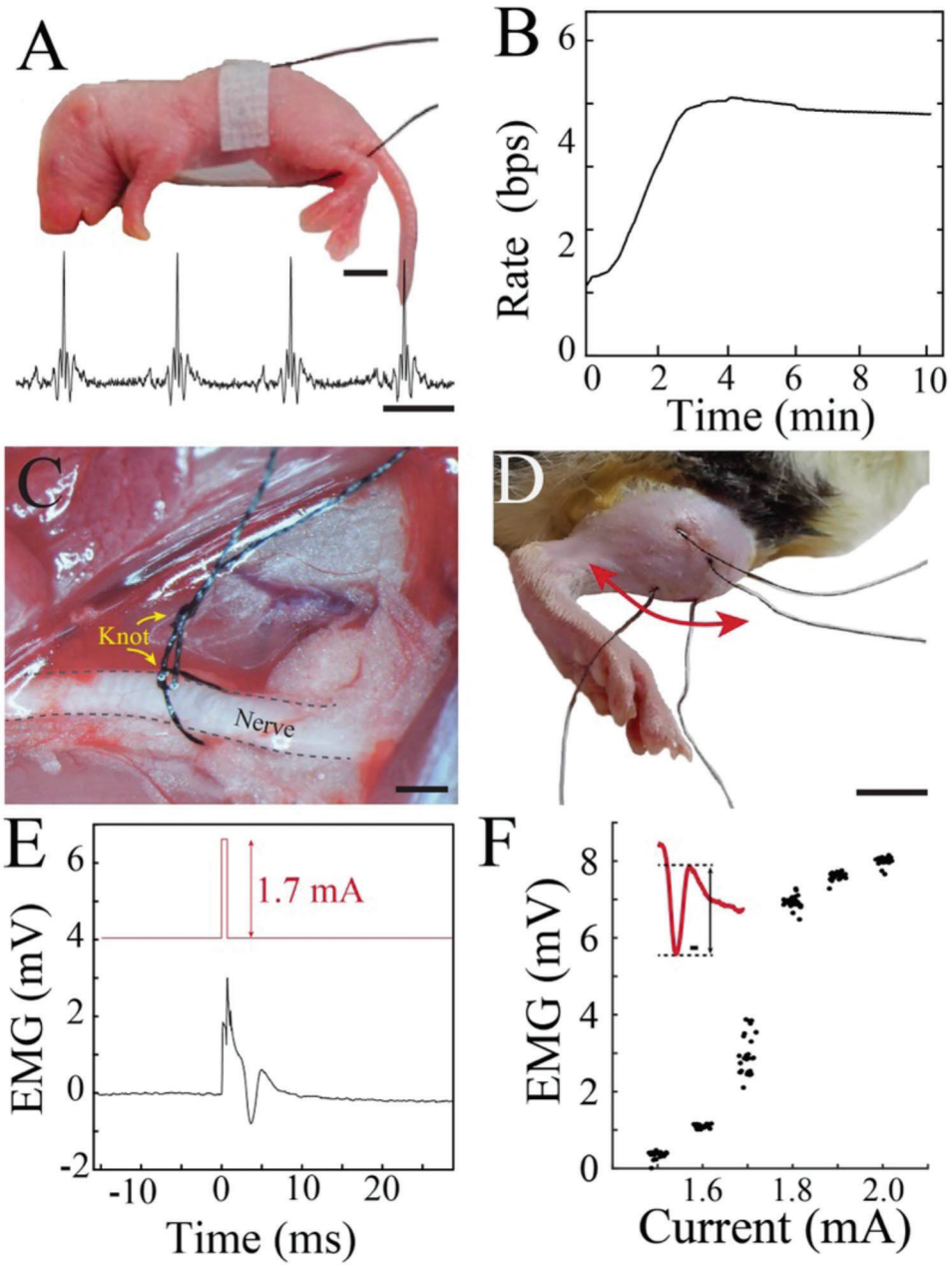

Figure 4. E-suture enables a minimally invasive electrophysiologic interface. A) Intra-operative photograph of e-suture-based ECG recording from a mouse pup at postnatal day 6 (upper; scale bar 2 mm). Sample ECG trace acquired by e-suture (lower; scale bar, 0.5 s). B) E-suture-based ECG recording tracks mouse pup heart rate during and throughout recovery from anesthesia. C) Intraoperative micrograph of an e-suture tied around the sciatic nerve to form a cuff electrode using a selectively uninsulated region of the suture for stimulation (Scale bar, 1 mm). D) Intraoperative micrograph of two pairs of stimulation and recording e-sutures inserted into the hindleg of an adult rat (Scale bar, 10 mm). E) Sample time trace of electrical pulse stimulation (1 ms duty cycle) and its corresponding EMG response recorded in an adult rat. F) Increase in EMG waveform amplitude as recorded by e-sutures functioning as differential recording electrodes with increasing current applied through e-sutures functioning as bipolar stimulating electrodes (n = 30 pulses per current level).

stereotactically implanted e-sutures onto the dorsal surface of the adult rat brain. Of note, the e-suture provided sufficient maneuverability to be inserted under the dura without requiring full dura removal across the entirety of the cranial window (**Figure** 5A). LFP recorded by the implanted e-suture permitted effective decoding of arousal state on the basis of oscillatory signals across delta (0.1–4 Hz), theta (6–10 Hz), and spindle (SPI; 10–20 Hz) frequency bands (Figure 5B). Consistent with known sleep and wake neural oscillations,[38–40] non-rapid eye movement sleep (NREM) contained prominent delta and spindle oscillations, whereas rapid eye movement sleep (REM) and mobility manifested continuous theta oscillations (Figure 5B;

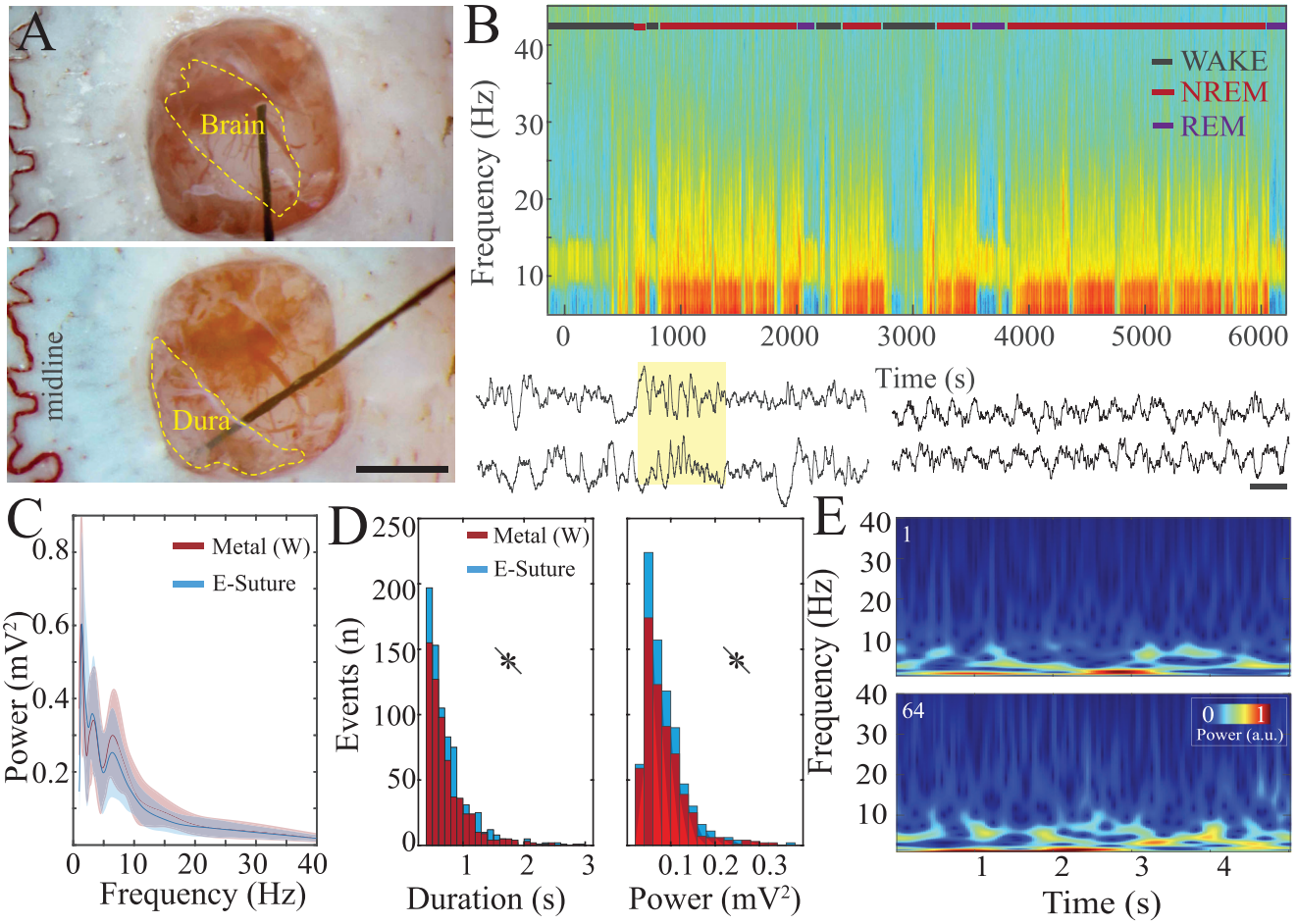

Figure 5. In vivo, chronic acquisition of neural activity enabled by e-sutures. A) Intraoperative micrograph of an e-suture implanted onto the pial surface of adult rat brain (top) and insertion of e-suture underneath the dura through a small dural incision (bottom). Scale bar 1 mm. B) Continuous time-frequency spectrogram of LFP recorded from an adult rat with an e-suture. Sleep states are overlaid in colored horizontal bars (top). Sample raw traces showing spindle events during NREM (bottom left, highlighted in yellow) and theta frequency during REM (bottom right) recorded with an e-suture (Scale bar 0.5 s). C) Analytic wavelet transform-derived power of 1–40 Hz activity acquired by e-suture (blue) and metal (red) electrodes from a 2 h LFP epoch (mean ± sd). D) Comparison of spindle event duration (left, $p = 0.61$, two-sample t-test) and peak power (right, $p = 0.94$, two-sample t-test) recorded with metallic surface electrode (red, $n = 616$) versus e-suture (blue, $n = 774$). E) Spectrograms of 1–40 Hz oscillatory power acquired by an e-suture electrode from two recordings nine weeks apart (top = day 1, bottom = day 64; 5 s window).

Figures S8–S10, Supporting Information). The power spectrum of data acquired by the e-suture, including at high frequencies, was comparable to that obtained by a conventional metallic microelectrode, indicating that the e-sutures appropriately sense and transmit neural signals (Figure 5C; Figure S10, Supporting Information). This notion was additionally supported by the ability of the e-suture to detect sleep spindles, which are key brain oscillations implicated in cognitive processes.[41–43] The duration and maximum power of spindles detected by e-sutures were comparable to those obtained using conventional cortical electrodes (Figure 5D).[44,45] Critically, the e-suture provided a high-quality long-term recording with no noticeable degradation in signal quality or decrease in the power of oscillatory patterns over the course of more than two months, highlighting its stability and biocompatibility (Figure 5E; Figure S9, Supporting Information). Finally, histological assessment of the brain tissue in the vicinity of e-sutures implanted for one week did not lead to significant cell loss (Figure S11, Supporting Information).

7. Conclusion

We demonstrated the potential for the e-suture to be deployed as a multifunctional bioelectronic component for a variety of electrophysiological procedures utilized in research and clinical applications, from sensing and stimulation to local drug delivery. Our fabrication approach generated e-sutures with highly conductive PEDOT:PSS-based cores and effective elastomer-based insulating jackets. The resultant structures were mechanically robust and demonstrated long-term stability in physiologic environments.

Because e-sutures could acquire high quality neurophysiologic data over the course of months in vivo, it is conceivable that e-sutures could provide sensing capacity across the conventional duration of non-dissolvable suture use in patients post-operatively (1–2 weeks). Such an approach could enable monitoring or stimulation of wound healing[46] as well as expedited neuromuscular recovery[47] without requiring implantation

of any additional components beyond those required for the initial surgical procedure. Based on current results, the biocompatibility and stability of e-sutures could also enable significantly longer-term implantation depending on clinical need.

E-sutures functioned as effective non-fluidic localized drug delivery devices. The mechanical flexibility of the composite materials and facile scalability of the length of the e-suture enable a diversity of device designs, which could loosen current restrictions on implantation of such systems. We anticipate that the drug delivery system could be used to target conditions ranging from seizure prophylaxis post-neurosurgery to localized post-surgical pain management.

Compared to previous research on bioelectronic wires and sutures that use similar materials and geometries,[46,48,49] the capabilities of our e-sutures demonstrated in this work expand the range of functions and potential target tissues of such technologies. E-sutures demonstrate chronic signal acquisition capacity with stability and quality similar to conventional metallic electrodes. They are also multifunctional, permitting sensing, stimulation and concurrent drug delivery. Combined with their softness, biocompatibility, electrical conductivity, and ease of integration with existing bioelectronics, e-sutures have the potential to simplify design of implantable devices and are broadly applicable to diagnostic and therapeutic applications that currently employ conventional sutures and wire interconnects.

8. Experimental Section

Material Preparation: PEDOT:PSS (Clevios PH1000) was purchased from Heraeus Epurio LLC. Surgical sutures were obtained from Amazon Inc. and Fisher Scientific (Ethicon, Braintree Scientific, CynaMed). (3-glycidyloxypropyl)trimethoxysilane (GOPS), 4-dodecyl benzene sulfonic acid (DBSA), 3-(trimethoxysilyl)propyl methacrylate (A-174 silane), polydimethylsiloxane (PDMS, Sylgard 184), ethylene glycol (EG), acetic acid and phosphate buffered saline (PBS) were purchased from Sigma-Aldrich. Parylene-C (Pa-C) was purchased from Special Coating Services. The conducting polymer mixture used for sutures contained 80% PH1000 and 20% EG with added 0.6% (v/v) DBSA and 0.5% (v/v) GOPS. The solution was mixed vigorously and then sonicated for 10 min before adding DBSA, for 10 min after addition DBSA and for another 10 min after addition of GOPS.

E-Suture Fabrication: The silk fibers were prepared by first rinsing in soapy water and flushing with DI water. Next, the fibers were immersed in acetone and sonicated for 10 min and afterward rinsed with DI water. The sonication was repeated with isopropyl alcohol. After a final DI rinse, the fibers were placed in an oven at 100 °C for 30 min to dry. After drying, the fibers were fully immersed in the PEDOT:PSS solution described above for 15 min. The fibers were then laid out on an aluminum sheet and baked at 100 °C for 15 min. This process was repeated at least 5 times. After the final PEDOT:PSS soak, the suture was baked at 100 °C for 1 h. Next, PDMS was mixed in a 10:1 ratio (elastomer: hardener) and applied to the suture along its length using a micro-applicator and then scrubbed to a thin layer with a cellulose-polyester (cleanroom) wipe. The PDMS was then cured by placing the suture in an oven at 100 °C for 1 h under vacuum. For Pa-C deposition, the PDMS coated suture was placed in a chemical vapor deposition system (Lab-Coater 2, Specialty Coating Systems). An adhesion promoter (Silane A-174, Sigma-Aldrich) was used in the deposition chamber to enhance Pa-C bonding. Any sections along the length of the suture that were intended to be unjacketed, e.g. mechanical connection sections for electrochemical measurements and ion pump hydration section, were shielded using Kapton tape to prevent PDMS and Pa-C contact.

Ion Pump Fabrication: E-suture channels for the ion pump were fabricated by leaving a ~5 cm section uninsulated at one end. The prototypic device used a 0.5 mL polypropylene centrifuge tube as a reservoir. The e-suture was incorporated by drilling a small hole in the tube bottom and then inserting the uninsulated portion to the inside of the tube while leaving the insulated portion extruding out for placement to the target. The hole was then sealed with PDMS under vacuum and allowed to cure for 24 h in room temperature. After sealing, the reservoir was filled with a solution containing the delivery chemical (a 2% aqueous solution of acetic acid or 1 M KCl) such that the e-suture inside the tube was fully immersed. The e-suture was allowed to hydrate in the solution for 24 h before use. For applying voltage to the system, an Ag/AgCl electrode was placed in the reservoir solution but with no ohmic contact to the e-suture. To establish an ohmic contact between the e-suture and the recording electrode for the e-suture-based ion pump with recording capacity (Figure 3A; Figure S7, Supporting Information), a ~1 cm section of the e-suture was left uninsulated near the tip to contact the target tissue. The contact was made using a single strand of an unwoven Litz wire with its insulation stripped from a ~3 cm section at one end. This uninsulated Litz wire section was wrapped tightly around the uninsulated e-suture segment to generate the ohmic contact and then fixed with PDMS. The wire was then connected to the recording system (see in vivo Procedures).

Scanning Electron Microscopy: All SEM images were taken using NovaNano SEM at Columbia Nano Initiative.

Electrical Characterization: Basic conduction properties and conductive polymer content of the e-sutures were determined by measuring the resistance across 1 cm of the PEDOT:PSS coated silk at multiple points along the length of the suture using a digital multimeter. The measurement contacts were made by clipping the suture to silver pins in a header with a fixed pitch using two toothless alligator clips. The ratio of PEDOT:PSS in the e-suture cross section was found by dividing the estimated cross-sectional area of PEDOT:PSS by that of the silk suture. For a size 4-0 silk suture, the standard diameter was 150 µm and for a size 7-0 suture the diameter was 50 µm, which corresponded to cross-sectional areas of 1.77×10^{-4} cm^2 and 1.96×10^{-5} cm^2, respectively.

Electrochemical Characterization: Electrochemical impedance spectroscopy measurements were performed using a potentiostat (Reference 600+, Gamry Instruments). The e-suture was immersed in a cell consisting of a bath of PBS, a counter electrode (Pt), and a reference electrode (Ag/AgCl). One or both ends of the suture were left outside of the cell for measuring the tip and the full-length e-suture impedance, respectively. The potentiostat working- and working sense electrodes were connected mechanically to one end of the e-suture outside of the cell. The potentiostatic EIS measurements were taken for a frequency range of 1 Hz – 10 kHz with 10 data points per decade. For lengthwise characterization of the insulation uniformity, the e-suture was pulled straight and suspended in the air horizontally. A 1 cc syringe was then filled with PBS and an Ag/AgCl electrode placed inside of it. The syringe was sealed from one end to maintain a PBS reservoir with a small droplet protruding from the opposite tip. This droplet was then placed on the suture and moved along its length with a separate EIS measurement taken at each point. The CE/REF electrodes were connected to the Ag/AgCl electrode in the PBS and the working electrode was connected to both tips of the e-suture that was left uninsulated for mechanical contacts.

Mechanical Characterization: Tensile strength of the e-suture was measured using a Nextech DFS50 force gauge. The sutures were fixed using knots and pulled vertically until breakage. The applied force over time was recorded using the Nex-Graph 3.4 software. The tested groups were plain silk-sutures, an unjacketed e-suture, a fully fabricated e-suture, and a plain nylon suture. All sutures were size 4-0.

In Vivo Procedures: All animal experimentation was approved by the Institutional Animal Care and Use Committee at Columbia University Irving Medical Center (Protocol No. AC-AABI5560 and AC-AABI5568).

For peripheral nervous system recording and stimulation, one male Long-Evans rat (300–350 g, Charles River) was anesthetized using isoflurane gas and placed on a stereotactic frame. Hair was removed from the hindleg and four e-sutures were inserted to the thigh muscle using a hypodermic needle as a cannula. Two sutures served as the positive and

negative electrodes for current delivery and the other two served as the recording and GND/REF electrode for EMG acquisition. For an additional GND electrode, we used an ECG electrode attached to the skin of the animal. Current delivery was performed using a STG4002 stimulus generator and the MC_Stimulus II Software (MultiChannel Systems Inc.) with 1 ms pulses delivered every 3 s at varying currents for 30 total pulses per current level. Concurrent EMG was recorded using the Intan RHD2000 (Intan Technologies) evaluation system with a sampling rate of 20 kHz.

For ECG recording, one male Swiss-Webster P6 mouse pup was anesthetized with hypothermia and anesthesia maintenance continued with gaseous isoflurane delivery. Two e-sutures, one for recording and one for GND/REF, were fixed onto the skin of the animal using surgical tape. ECG was recorded using the Intan RHD2000 evaluation system with a sampling rate of 20 kHz. Recording was performed continuously under anesthesia and throughout recovery from anesthesia.

For chronic neural recordings, one male Long-Evans rat (300–350 g, Charles River) was anesthetized using isoflurane gas and placed in a stereotactic frame for intracranial placement of e-sutures and metal electrodes. Burr holes for e-suture insertion were drilled over the right cerebral hemisphere, between the lamboid and the coronal sutures. (AP: – 2 mm and – 4 mm, ML: +3 mm). The dura was excised prior to lowering the suture tip stereotactically onto the surface of the brain. A microelectrode array consisting of five 50 µm diameter tungsten (W) wires spaced 50 µm from each other was implanted onto the contralateral side for comparison (AP: – 3.5 mm, ML: – 3 mm, DV: – 1 mm) with a craniotomy size of 1.5 × 1.5 mm^2. The craniotomies were sealed with a hemostatic sponge (Gelfoam, Pfizer Inc.) and a biocompatible silicone encapsulant (Kwik-Sil, WPI Inc.) Two additional burr holes were drilled over the cerebellum for insertion of stainless-steel screws to serve as ground and reference electrodes. A shielding structure made of copper (Cu) mesh and an acrylic resin (UNIFAST Trad) was then built around the implants. After a week of post-surgical recovery, LFP was recorded weekly from the animal using the Intan RHD2000 evaluation system up to 9 weeks. Channels were sampled at 20 kHz.

For e-suture based ion pump system testing, one male Long-Evans rat (300–350 g, Charles River) was anesthetized using isoflurane gas and placed on a stereotactic frame for intracranial placement of the ion-pump device and metal electrodes. 1 × 1 mm^2 craniotomies were drilled over the right cerebral hemisphere at AP: – 2 mm, ML: +3 mm; AP: – 4 mm, ML: +1.5 mm and AP: – 4 mm, ML: +3.5 mm for the metallic (W) electrodes, the e-suture counter electrode and the e-suture ion pump, respectively. Following dura removal, the implants (a microelectrode array of two 50 µm tungsten wires with a spacing of 50 µm, a counter e-suture, and the e-suture ion pump) were placed in direct contact with the exposed cortical surface in their respective craniotomies. Two burr holes were drilled over the cerebellum for epidural insertion of GND/REF stainless steel screws. The two tungsten electrodes and the electrical sensing wire on the e-suture ion pump (see Ion Pump Fabrication – section) were connected to a 32-channel Intan RHD2000 preamplifier. The intraoperative recordings were performed using the Intan RHD2000 evaluation system with a sampling rate of 20 kHz. The recordings comprised of three epochs: i) baseline prior to pump activation; ii) pump activation; iii) recovery after pump inactivation. To turn the pump on, a 9 V battery was connected between the counter e-suture and an Ag/AgCl electrode inside the solution reservoir of the ion-pump. Current was monitored using a digital multimeter unit with readings every 10 s.

To assess biocompatibility of the e-suture implants in neural tissue, one female Long-Evans rat (200–250 g, Charles River) was anesthetized using isoflurane and placed on a stereotaxic frame. Four burr holes were drilled at AP: – 2 mm, ML: ± 3 mm & AP – 4 mm, ML ± 3 mm, the dura removed and the e-sutures placed in contact with the cortical surface. The craniotomies were sealed with a hemostatic sponge (Gelfoam, Pfizer Inc.) and a biocompatible silicone encapsulant (Kwik-Sil, WPI Inc.) A shielding structure made of copper mesh and an acrylic resin (UNIFAST Trad) was then built around the implants. At seven days post-implantation the animal was euthanized.

Tissue Response Histology: After euthanasia, the animal was immediately perfused with PBS and 4% paraformaldehyde (PFA) followed by brain extraction and 48 h of post-fixation in 4% PFA. After fixation, the brain was immersed in PBS and sliced coronally using a vibratome (Leica vt1000s) at 80 µm. The slices were then incubated with DAPI (D9542-5MG; Sigma-Aldrich) at 0.2 µg mL^{-1} and mounted to slides with Fluoromount-G (00-4958-02, ThermoFisher). Fluorescent images were captured and tiled using a computer-assisted camera connected to an ECHO Revolve microscope. The images were adjusted for brightness and contrast and assembled into panels using ImageJ and Adobe Illustrator. Cell counts were determined from cortical layer I at the vicinity of e-suture implantation and at adjacent sites for comparison by adjusting for brightness/contrast, thresholding and then using the "Analyze Particles" – function of ImageJ.

Electrophysiological Data Analysis: Data visualization was performed using NeuroScope[50] and analysis was performed in MATLAB (MathWorks Inc.). All channels from all recordings were first resampled from 20 kHz to 1250 Hz. EMG and ECG data was also filtered using a Butterworth IIR filter with order n = 2 to remove ambient 60 Hz noise. Heart rate (in beats per second) was determined from the ECG data by detecting the R peak of the QRS complex using thresholding and calculating the local rate using a sliding window. EMG magnitude was calculated by detecting local maxima and minima within a 4 ms window centered at 5 ms post-stimulus and calculating total waveform amplitude as the difference between these values.

Chronic neural recordings were assigned arousal states (wakefulness, non-REM or REM sleep) for each second of recording based on relative delta (0.5–4 Hz) and theta (6–10 Hz) frequency band power, as well as the accelerometer signal amplitude. Spindle detection was performed by bandpass filtering the raw trace during non-REM sleep at 10–20 Hz followed by thresholding the normalized signal squared using the standard deviation (sd) of the signal. Events were determined to start and stop at times when the signal crossed 2 × sd and were discarded if a peak at above 3 × sd did not occur during the start-stop interval. Events deemed too long (> 3 s) or short (< 300 ms) were discarded and events having an insufficient inter-event latency (< 400 ms) were merged and reassessed for length. The detection was verified by visually inspecting the detected events. The properties of spindles detected with a cortical surface electrode and an e-suture were compared by calculating the histograms of spindle duration and peak power for both recording electrode types. The statistical significance of the difference between spindles recorded with the two electrode types was assessed using a two-sample t-test. Overall power spectral content in the LFP recorded from tungsten wires and e-sutures was assessed using analytic wavelet transforms in 5 s non-overlapping windows along the length of the recording with a frequency range of 1–40 Hz at 0.05 Hz resolution. For power spectral analysis, the recordings were resampled to the Nyquist frequency of the desired maximum frequency of analysis and then split into non-overlapping 5 s windows. An analytic Gabor wavelet transformation using a frequency resolution of 0.05 Hz was then performed on each individual window, and finally the windows were summed to derive the power spectrum for an entire recording. For whitened spectrograms, whitening was performed prior to resampling using Burgs method with order n = 1.

Intraoperative ion pump data was analyzed to characterize the introduction of epileptic sharp waves and spikes by quantifying the z-score of the negative portion of the first derivative of the signal. Outliers (< 0.01% and > 99%) of the z-scored data, representing the episodic occurrence of sharp waveforms, were compared between the baseline, pump activation, and post-pump inactivation recording epochs.

Statistical Analysis: All statistical analysis was performed using MATLAB (MathWorks Inc.). For omnibus tests, either one-way or Kruskal-Wallis ANOVA tests were performed, which were followed up by Dunn-Sidak post hoc correction for multiple comparisons using built-in MATLAB functions. For direct comparisons, t-tests or two-sample t-tests were used.

Supporting Information

Supporting Information is available from the Wiley Online Library or from the author.

Acknowledgements

This work was supported by Columbia University, School of Engineering and Applied Science as well as Columbia University Medical Center, Department of Neurology. The device fabrication was performed at Columbia Nano-Initiative. This work was supported by the National Institutes of Health grants R01NS118091, R21 EY 32381-01, RF1NS128669, National Science Foundation 1944415 and 2219891. The authors would like to thank J. Vichiconti, Y. Borisenkov, P. Chow, C. Belfer, N. Ariel-Sternberg (CNI), D. Tukey and J. Wang (Pallas Technologies) and all Khodagholy and Gelinas laboratory members for their support.

Conflict of Interest

The authors declare no conflict of interest.

Author Contributions

DK and JNG conceived the project. OJR and DK designed, developed, fabricated, and characterized material and devices. DJW, MK, and ZZ contributed to testing and fabrication of sutures. SS, JF, and BS contributed to histological and biocompatibility experiments. OJR, LM, DK, and JNG did the electrophysiology in vivo rodent experiments and analysis. All authors contributed to writing the paper.

Data Availability Statement

The data that support the findings of this study are available from the corresponding author upon reasonable request.

Keywords

biocompatible materials, conducting polymers, implantable electronics, neural interface devices, organic bioelectronics, silk

Received: August 9, 2023
Revised: December 17, 2023
Published online: January 14, 2024

[1] I. Willner, E. Katz, *Bioelectronics: From Theory to Applications*, Wiley-VCH, Weinheim **2005**.
[2] K. Birmingham, V. Gradinaru, P. Anikeeva, W. M. Grill, V. Pikov, B. Mclaughlin, P. Pasricha, D. Weber, K. Ludwig, *Nat. Rev. Drug Discov.* **2014**, *13*, 399.
[3] E. Krook-Magnuson, J. N. Gelinas, I. Soltesz, G. Buzsáki, *JAMA Neurol.* **2015**, *72*, 823.
[4] R. S. Sanders, M. T. Lee, *Proc. IEEE* **1996**, *84*, 480.
[5] B. Lee, M. N. Zubair, Y. D. Marquez, D. M. Lee, L. A. Kalayjian, C. N. Heck, C. Y. Liu, *World Neurosurg.* **2015**, *84*, 719.
[6] R. L. Johnson, C. G. Wilson, *J. Inflamm. Res.* **2018**, *11*, 203.
[7] J. S. Perlmutter, J. W. Mink, *Annu. Rev. Neurosci.* **2006**, *29*, 229.
[8] P. Jastrzebska-Perfect, S. Chowdhury, G. D. Spyropoulos, Z. Zhao, C. Cea, J. N. Gelinas, D. Khodagholy, *Adv. Funct. Mater.* **2020**, *30*, 1909165.
[9] D. Khodagholy, J. J. Ferrero, J. Park, Z. Zhao, J. N. Gelinas, *Trends Neurosci.* **2022**, *45*, 968.
[10] D. Benninger, M. Schüpbach, *Ther. Umsch.* **2018**, *75*, 425.
[11] Z. Zhao, C. Cea, J. N. Gelinas, D. Khodagholy, *Proc. Natl. Acad. Sci. USA* **2021**, *118*, e2022659118.
[12] G. Findikoglu, B. S. Yildiz, M. Sanlialp, Y. I. Alihanoglu, I. D. Kilic, H. Evregul, H. Senol, *Int. J. Rehabil. Res.* **2015**, *38*, 287.
[13] E. F. F. Chang, *Neuron* **2015**, *86*, 68.
[14] M. Berggren, A. Richter-Dahlfors, *Adv. Mater.* **2007**, *19*, 3201.
[15] A. Jonsson, Z. Song, D. Nilsson, B. A. Meyerson, D. T. Simon, B. Linderoth, M. Berggren, *Sci. Adv.* **2015**, *1*, e1500039.
[16] J. Rivnay, R. M. Owens, G. G. Malliaras, *Chem. Mater.* **2014**, *26*, 679.
[17] C. M. Proctor, A. Slézia, A. Kaszas, A. Ghestem, I. del Agua, A. M. Pappa, C. Bernard, A. Williamson, G. G. Malliaras, *Sci. Adv.* **2018**, *4*.
[18] D. T. Simon, S. Kurup, K. C. Larsson, R. Hori, K. Tybrandt, M. Goiny, E. W. H. Jager, M. Berggren, B. Canlon, A. Richter-Dahlfors, *Nat. Mater.* **2009**, *8*, 742.
[19] J. Isaksson, P. Kjäll, D. Nilsson, N. D. Robinson, M. Berggren, A. Richter-Dahlfors, *Nat. Mater.* **2007**, *6*, 673.
[20] I. Uguz, C. M. Proctor, V. F. Curto, A.-M. Pappa, M. J. Donahue, M. Ferro, R. M. Owens, D. Khodagholy, S. Inal, G. G. Malliaras, *Adv. Mater.* **2017**, *29*.
[21] O. Dadras-Toussi, M. Khorrami, A. S. C. Louis Sam Titus, S. Majd, C. Mohan, M. R. Abidian, *Adv. Mater.* **2022**, *34*, 2200512.
[22] K. Tybrandt, D. Khodagholy, B. Dielacher, F. Stauffer, A. F. Renz, G. Buzsáki, J. Vörös, *Adv. Mater.* **2018**, *30*, 1706520.
[23] D. Khodagholy, J. N. Gelinas, T. Thesen, W. Doyle, O. Devinsky, G. G. Malliaras, G. Buzsáki, *Nat. Neurosci.* **2015**, *18*, 310.
[24] D. Khodagholy, J. Rivnay, M. Sessolo, M. Gurfinkel, P. Leleux, L. H. Jimison, E. Stavrinidou, T. Herve, S. Sanaur, R. M. Owens, G. G. Malliaras, *Nat. Commun.* **2013**, *4*, 2133.
[25] J. Rivnay, P. Leleux, M. Ferro, M. Sessolo, A. Williamson, D. A. Koutsouras, D. Khodagholy, M. Ramuz, X. Strakosas, R. M. Owens, C. Benar, J.-M. Badier, C. Bernard, G. G. Malliaras, *Sci. Adv.* **2015**, *1*, 140025.
[26] E. Stavrinidou, P. Leleux, H. Rajaona, D. Khodagholy, J. Rivnay, M. Lindau, S. Sanaur, G. G. Malliaras, *Adv. Mater.* **2013**, *25*, 4488.
[27] D. A. Koutsouras, P. Gkoupidenis, C. Stolz, V. Subramanian, G. G. Malliaras, D. C. Martin, *ChemElectroChem* **2017**, *4*, 2321.
[28] A. R. Hassan, Z. Zhao, J. J. Ferrero, C. Cea, P. Jastrzebska-Perfect, J. Myers, P. Asman, N. F. Ince, G. McKhann, A. Viswanathan, S. A. Sheth, D. Khodagholy, J. N. Gelinas, *Adv. Sci.* **2022**, *9*, 2202306.
[29] D. Khodagholy, J. N. Gelinas, Z. Zhao, M. Yeh, M. Long, J. D. Greenlee, W. Doyle, O. Devinsky, G. Buzsáki, *Sci. Adv.* **2016**, *2*.
[30] R. Green, M. R. Abidian, *Adv. Mater.* **2015**, *27*, 7620.
[31] M. R. Abidian, D. C. Martin, *Adv. Funct. Mater.* **2009**, *19*, 573.
[32] M. R. Abidian, D. C. Martin, *Biomaterials* **2008**, *29*, 1273.
[33] M. R. Abidian, K. a. Ludwig, T. C. Marzullo, D. C. Martin, D. R. Kipke, *Adv. Mater.* **2009**, *21*, 3764.
[34] G. H. Altman, F. Diaz, C. Jakuba, T. Calabro, R. L. Horan, J. Chen, H. Lu, J. Richmond, D. L. Kaplan, *Biomaterials* **2003**, *24*, 401.
[35] D.-H. Kim, J. Viventi, J. J. Amsden, J. Xiao, L. Vigeland, Y.-S. Kim, J. a. Blanco, B. Panilaitis, E. S. Frechette, D. Contreras, D. L. Kaplan, F. G. Omenetto, Y. Huang, K.-C. Hwang, M. R. Zakin, B. Litt, J. a Rogers, *Nat. Mater.* **2010**, *9*, 511.
[36] Z. Jia, J. Gong, Y. Zeng, J. Ran, J. Liu, K. Wang, C. Xie, X. Lu, J. Wang, *Adv. Funct. Mater.* **2021**, *31*, 2010461.
[37] S. Domínguez, L. Ma, H. Yu, G. Pouchelon, C. Mayer, G. D. Spyropoulos, C. Cea, G. Buzsáki, G. Fishell, D. Khodagholy, J. N. Gelinas, *Elife* **2021**, 10.
[38] Y. Nir, R. J. Staba, T. Andrillon, V. v. Vyazovskiy, C. Cirelli, I. Fried, G. Tononi, *Neuron* **2011**, *70*, 153.
[39] G. Buzsaki, *Neuron* **2002**, *33*, 325.
[40] G. Buzsáki, A. Draguhn, *Science* **2004**, *304*, 1926.
[41] G. Buzsáki, *Neuroscience* **1989**, *31*, 551.
[42] D. Khodagholy, J. N. Gelinas, G. Buzsáki, *Science* **2017**, *358*, 369.
[43] N. Maingret, G. Girardeau, R. Todorova, M. Goutierre, M. Zugaro, *Nat. Neurosci.* **2016**, *19*, 959.

[44] J. N. Gelinas, D. Khodagholy, T. Thesen, O. Devinsky, G. Buzsáki, *Nat. Med.* **2016**, *22*, 641.
[45] P. Dahal, N. Ghani, A. Flinker, P. Dugan, D. Friedman, W. Doyle, O. Devinsky, D. Khodagholy, J. N. Gelinas, *Brain* **2019**, *142*.
[46] V. Kalidasan, X. Yang, Z. Xiong, R. R. Li, H. Yao, H. Godaba, S. Obuobi, P. Singh, X. Guan, X. Tian, S. A. Kurt, Z. Li, D. Mukherjee, R. Rajarethinam, C. S. Chong, J. W. Wang, P. L. R. Ee, W. Loke, B. C. K. Tee, J. Ouyang, C. J. Charles, J. S. Ho, *Nat. Biomed. Eng.* **2021**, *5*, 1217.
[47] J. Lee, S. J. Ihle, G. S. Pellegrino, H. Kim, J. Yea, C. Y. Jeon, H. C. Son, C. Jin, D. Eberli, F. Schmid, B. L. Zambrano, A. F. Renz, C. Forró, H. Choi, K. I. Jang, R. Küng, J. Vörös, *Nat. Electron.* **2021**, *4*, 291.
[48] S. Watanabe, H. Takahashi, K. Torimitsu, *Jpn. J. Appl. Phys.* **2017**, *56*.
[49] J. Lee, S. J. Ihle, G. S. Pellegrino, H. Kim, J. Yea, C. Y. Jeon, H. C. Son, C. Jin, D. Eberli, F. Schmid, B. L. Zambrano, A. F. Renz, C. Forró, H. Choi, K. I. Jang, R. Küng, J. Vörös, *Nat. Electron.* **2021**, *4*, 291.
[50] L. Hazan, M. Zugaro, G. Buzsáki, *J. Neurosci. Methods* **2006**, *155*, 207.